Interreg North Sea

Co-funded by the European Union

WaterWarmth

WORKPACKAGE 4

Smart integration of Aquathermal Energy into the local energy system

4.6 Disseminating results on system integration to local actors and to the scientific community

PV–Battery Powered Surface Water Heat Pump System Control and Simulation

Version December 2025

Joyce Assaf , Mamadou-Baïlo Camara , Damien Guilbert , Brayima Dakyo Groupe de Recherche en Electrotechnique et Automatique du Havre (GREAH) Université Le Havre Normandie

ACCELERATING THE TRANSITION TOWARDS SUSTAINABLE HEATING AND COOLING BASED ON COLLECTIVE SURFACE WATER HEAT PUMP SYSTEM

Interreg North Sea
Co-funded by the European Union
WaterWarmth

PV–Battery Powered Surface Water Heat Pump System Control and Simulation

Joyce Assaf, Mamadou-Baïlo Camara, Damien Guilbert, Brayima Dakyo
Groupe de Recherche en Electrotechnique et Automatique du Havre (GREAH)
Université Le Havre Normandie
Le Havre, Normandie, France
e-mail: joyce.assaf@univ-lehavre.fr, camaram@univ-lehavre.fr, damien.guilbert@univ-lehavre.fr, brayima.dakyo@univ-lehavre.fr

***Abstract*—This paper presents the modeling, control strategy, and simulation of a hybrid energy system comprising a 31 kW photovoltaic (PV) array, a 35 kWh battery energy storage system (BESS), and two parallel 30 kW surface water heat pumps (SWHPs), all interconnected through a DC–link. The designed system supports the energy needs of an aquathermal energy (AE) harvesting pilot site under development in 'Le Cano Ouistreham', Normandie, France, as part of the 'Waterwarmth' project, funded by Interreg North Sea Region. Customized maximum power point tracking (MPPT) and BESS control strategies were implemented on their respective converters to ensure efficient PV energy harvesting and stable power supply to the SWHPs. The simulation results demonstrate the effectiveness of coupling the electrical and thermal sectors to decarbonize heating.**

Keywords-Photovoltaics; surface water heat pump; battery energy storage system; control strategy; energy management.

I. Introduction

The heating sector represents a significant portion of global final energy consumption and remains heavily reliant on fossil fuels. Around 10% of the global demand for space heating was met by heat pumps (HPs) in 2021, and installations are accelerating, with nearly 30 million new units expected to be installed by 2030 in the European Union [1]. HPs use the same technology found in refrigerators and air conditioners: they extract heat from a low temperature source, such as ambient air, groundwater, wastewater, or surface water, and transfer it to a higher temperature sink to provide domestic hot water or space heating/cooling.

A surface water heat pump (SWHP) recovers heat from various surface water sources such as seawater, lake water, and river water to meet the heating demand. In recent years, SWHPs have gained significant attention, as surface water thermal energy can supply more than 40% of the heat demand in buildings [2]. Despite this potential, large-scale deployment of HPs faces integration challenges [3]. At the same time, powering the SWHP compressor from renewable energy sources (RESs) is crucial to decarbonizing the heating sector, as nearly 90% of district heat globally was still produced from fossil fuels in 2022 [4].

In this context, hybrid systems combining photovoltaic (PV) arrays, battery energy storage systems (BESSs), and SWHPs are emerging as sustainable and self-sufficient solutions for thermal energy supply. Although numerous simulations of such systems can be found in the literature [5]–[7], most provide limited information on the detailed modeling of power electronics that interface the supply and demand sides. Additionally, aspects such as DC–bus voltage dynamics and energy management strategies needed to maintain system stability under varying environmental and load conditions are often inadequately addressed. This represents a notable gap in current research on SWHP integration with RESs.

Recent advances have focused on improving individual components. For instance, the authors in [8] proposed a high-voltage DC–DC converter for a 76 kW PV system that powers a 55 kW HP, achieving a voltage gain four times higher at 0.5 duty cycle compared to conventional converters. Another study introduced a model predictive control strategy for a PV–SWHP system without accounting for the dynamic load profile of the SWHP [9]. Alternatively, in [10], the authors developed an adaptive nonlinear fractional order proportional–integral–derivative (PID) maximum power point tracking (MPPT) controller that adjusts gains in real time and uses fractional calculus for higher precision. Using the Lambert-W function for explicit PV array modeling, their method achieved a tracking efficiency of 99.38%, outperforming conventional PID (99.05%) and adaptive non-linear PID (98.79%) controllers, even under partial shading and rapidly changing irradiance conditions. However, this work is limited to the PV–converter subsystem and does not address system-level integration with BESS or dynamic loads.

To address these gaps, this paper presents the detailed modeling, control design, and simulation of a hybrid energy system comprising a 31 kW PV array, a 35 kWh lithium-ion BESS, and two parallel 30 kW SWHPs. All components are interconnected through a common DC–link and coordinated through customized MPPT and battery management algorithms. The system is designed to meet the thermal needs of 'Le Cano Ouistreham' pilot site in Normandie, France, in the context of the Interreg-funded 'Waterwarmth' project.

In contrast to previous studies, this work combines high-resolution thermal load data with detailed power electronics modeling to evaluate system stability under realistic climatic and demand variations.

This paper makes the following key contributions:

- Simulation of a full hybrid PV–BESS–SWHPs system under realistic climatic and thermal demand conditions;
- Modified incremental conductance (INC) MPPT algorithm with adaptive step size and threshold control for faster and more accurate PV power tracking;
- Dual-loop control of the BESS converter to maintain DC–bus voltage stability and ensure dynamic power flow balancing;

- Detailed performance analysis of the system's electrical and thermal interactions, demonstrating suitability for decarbonized heating applications.

The remainder of this paper is organized as follows: Section II describes the system configuration and modeling approach. Section III details the control strategies implemented for the PV and BESS subsystems. Section IV presents the simulation results. Finally, Section V concludes the paper and outlines directions for future work.

II. SYSTEM CONFIGURATION

The proposed hybrid system integrates a PV array, a BESS, and two SWHPs, all interconnected through a common DC–link. The overall electrical architecture is illustrated in Fig. 1, which highlights the main components and their power electronic interfaces. This configuration ensures coordinated operation between generation, storage, and thermal demand.

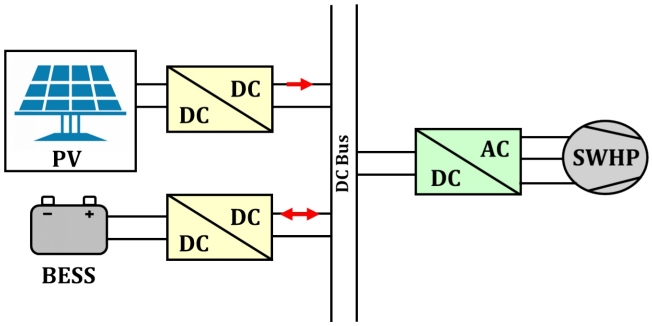

Fig. 1. Electrical schematic of the system.

A. Photovoltaic array

The PV subsystem consists of 11 parallel strings, each containing 8 Canadian Solar Inc. CS6X-350M-FG modules connected in series. The simulation uses measured irradiance and temperature data collected at the 'Le Cano Ouistreham' pilot site in Normandie, France. These measurements, illustrated in Fig. 2, span from March 7, 2024, at 11:00 AM to May 7, 2024, at 2:00 AM, with a sample time of one hour.

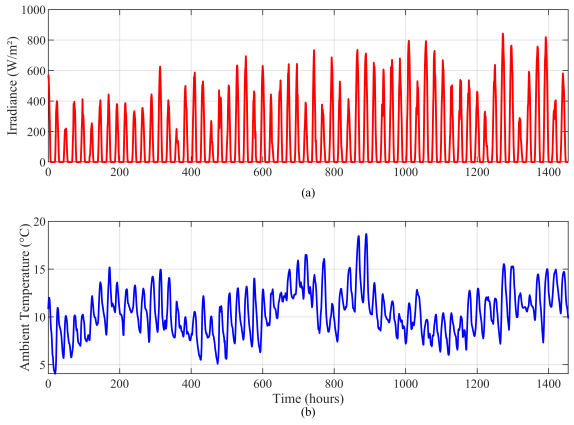

Fig. 2. Profiles of (a) irradiance; and (b) ambient temperature in 'Le Cano Ouistreham', Normandie, France.

During this period, the irradiance values ranged from 0, due to night or cloudy conditions, to 841.8 W/m^2, with a mean of approximately 155.7 W/m^2, reflecting typical solar availability in the region. The ambient temperatures ranged between 4.04 °C and 18.68 °C, with an average of 10.5 °C. These conditions provide a realistic foundation for evaluating the performance of the PV system in varying weather scenarios.

B. Battery Energy Storage System

Due to the intermittent nature of PV generation, the BESS is integrated into the system to maintain DC–bus voltage stability and ensure reliable operation under fluctuating renewable generation and load demand. The battery pack has a nominal voltage of 350 V and a rated capacity of 100 Ah, equivalent to 35 kWh. A bidirectional buck–boost converter interfaces the BESS with the DC–bus, allowing for both charging and discharging modes. This enables excess PV energy to be stored during high generation periods and released to support the load when PV output is insufficient. The control logic of this converter is explained in Section III.

C. Surface Water Heat Pump

The thermal load in the model is represented by two identical SWHP units connected in parallel. This arrangement aligns total electrical consumption with the nominal output of renewable generation and storage (31 kW PV coupled with a 35 kWh BESS). By satisfying the building's heating requirements, the configuration eliminates dependence on conventional fossil fuel-based backup systems, ensuring that the heating demand is met entirely through RESs. The SWHP model used in the simulation is a CIAT DYNACIAT LG 300 A water-to-water HP. It delivers a nominal heat capacity of 90.3 kW and a cooling capacity of 61.5 kW, with a rated electrical consumption of 29.4 kW.

The primary inputs of the model were the thermal power generated by the SWHPs and their coefficient of performance (COP), based on measurements of an installed system at an operational site in 'Dijlemolens', Belgium. This site also uses a backup gas boiler to satisfy the total building heat demand. The data covers the period from March 7, 2024 at 11:00 AM to May 7, 2024 at 2:00 AM, with a sample time of five seconds. The electrical power consumption for the two SWHPs is calculated based on the thermal load profile of the building, as well as the SWHP datasheet. It is given by (1):

$$P_{\text{elec,SWHP}} = \frac{P_{\text{thermal}}}{COP} \tag{1}$$

As shown in Fig. 3, the thermal load profile exhibits frequent peaks in high demand and varying on/off cycles, reflecting realistic building heating demand. Operating in a fully demand-driven mode, these dynamics emphasize the importance of a rapid control response from the supply side and a robust power balance between generation, storage, and load.

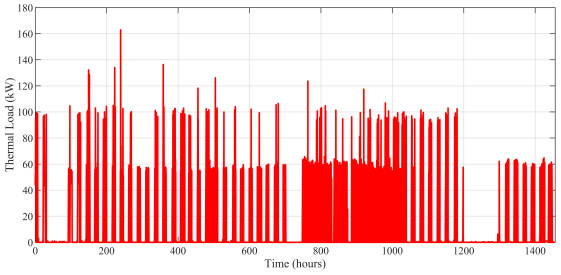

Fig. 3. Thermal load profile of the two SWHP units.

D. DC–DC Boost Converter for the PV array

In renewable energy systems that deliver a relatively low DC voltage at their source terminals, a step-up (boost) converter is typically used to elevate this voltage to match the DC–bus operating level [11]. In this study, the DC–bus voltage reference is set to 1000 V, which is typical for many RE applications, to ensure compatibility with industrial inverters and BESSs. The converter raises the PV generated voltage to the DC–bus voltage level, enabling efficient energy transfer under fluctuating ambient air temperature and irradiance conditions.

Various DC–DC converter topologies are found in the literature, each with trade-offs in efficiency, control complexity, and component stress, depending on the application requirement [12]. The DC–DC boost topology used in this study is illustrated in Fig. 4, to validate the working principles of the overall system, providing a solid foundation for further extension and refinement.

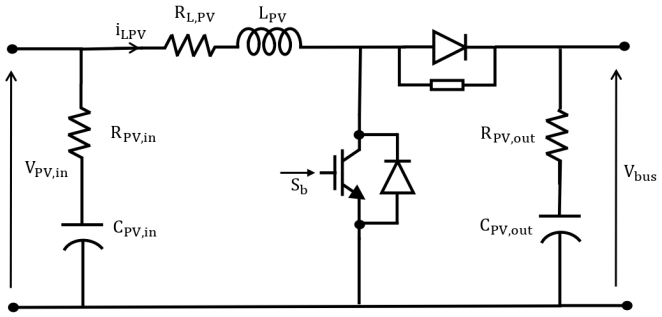

Fig. 4. Topology of the PV DC–DC boost converter.

In this configuration, the inductor current is calculated from (2) [13]. During the 'ON' state, the switch is closed and the duty cycle α = 1. In contrast, during the 'OFF' state, the switch is open and the duty cycle α = 0.

$$\frac{di_{\mathrm{LPV}}}{dt} = \frac{1}{L}\left[V_{\mathrm{PV,in}} - R_{\mathrm{L,PV}}\, i_{\mathrm{LPV}} - V_{\mathrm{bus}}(1-\alpha)\right] \qquad (2)$$

where $i_{L,PV}$ is the PV inductor current and $R_{L,PV}$ is the inductor resistance.

E. DC–DC Bidirectional Converter for the BESS

A bidirectional buck–boost converter interfaces the BESS with the DC–bus, allowing both charging and discharging modes to preserve voltage stability under varying load and generation conditions. During periods of high generation, it operates in buck mode to store excess energy in the battery. In contrast, when the generation drops below demand, it switches to boost mode to supply power from the battery to the load. This feature enables an effective energy balance between generation and demand and ensures a constant and reliable power supply under varying environmental conditions and load demands. Related HP studies including BESSs have been reported in the literature [14], [15]. The bidirectional converter topology adopted in this study is illustrated in Fig. 5 [16].

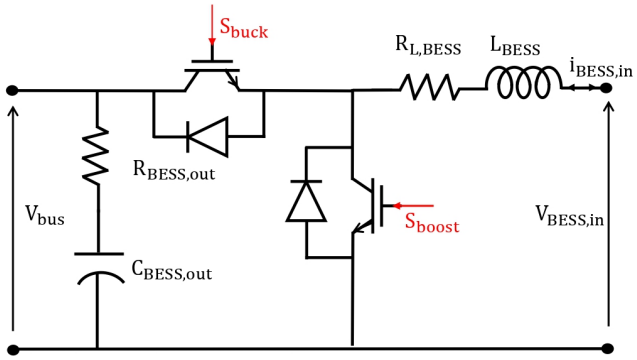

Fig. 5. Topology of the BESS bidirectional DC–DC converter.

The equations governing the working principle of the buck and boost modes of this bidirectional converter are presented in (3) [17].

$$\begin{cases} \dfrac{di_{\mathrm{BESS,in}}}{dt} = \dfrac{V_{\mathrm{BESS,in}} - V_{\mathrm{bus},S_{\mathrm{boost}}}}{L_{\mathrm{BESS}}} \\ \dfrac{dV_{\mathrm{bus}}}{dt} = \dfrac{i_{\mathrm{BESS},S_{\mathrm{buck}}} - i_{\mathrm{bus}}}{C_{\mathrm{BESS,out}}} \end{cases} \qquad (3)$$

where $i_{\mathrm{BESS,in}}$ represents the current exchanged with the battery, accounting for both charging and discharging modes, V_{bus} is the measured DC–bus voltage, S_{boost} and S_{buck} are the switching signals generated by the control algorithm described in Section III, L_{BESS} is the inductance of the boost converter, and $C_{\mathrm{BESS,out}}$ corresponds to the capacitor located at the output of the BESS, on the DC–bus side.

III. MICROGRID CONTROL METHODS

A. PV Boost Converter Control Strategy

The PV array is interfaced with the DC–bus through a unidirectional boost converter governed by an incremental conductance (INC) MPPT algorithm [18]. This approach determines the instantaneous slope of the PV I–V curve and compares it with the negative instantaneous conductance to locate the MPPT. Then, it dynamically regulates its duty cycle, ensuring operation at the MPPT under rapid irradiance or temperature variations. The algorithm begins with an initial duty cycle of 0.5 and sets upper and lower bounds between 0.25 and 0.95 to prevent overdriving the converter.

Unlike conventional INC methods that use fixed step sizes, this modified approach dynamically scales the duty cycle increment based on the magnitude of power changes, allowing

for faster convergence and reduced oscillations near the MPPT. The control logic compares instantaneous variations in voltage, current, and power to determine the direction of adjustment, with duty cycle updates triggered only when power changes exceed a predefined threshold.

Additionally, when solar irradiance drops to zero, the duty cycle is safely reset to zero to disable power conversion. The output of the algorithm, combined with the average current reference estimated from the irradiance, generates the total reference current for the PI-based current control, driving the PWM switching of the PV-side DC–DC converter. This ensures stable and optimal operation of the PV subsystem. The PWM control signal is shown in Fig. 6.

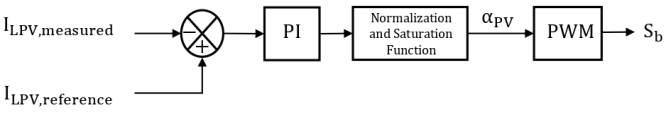

Fig. 6. PWM control signal of the PV boost converter switch.

B. BESS Bidirectional Converter Control Strategy

The BESS bidirectional converter control maintains the DC–bus voltage at 1000 V and manages the power flow direction (buck/boost) based on the instantaneous power balance. Accordingly, a dual-loop scheme with outer DC–bus regulation and inner current tracking was developed. The outer control loop regulates the DC–bus voltage by generating a current reference, while an inner loop ensures precise tracking of this current. The control logic is illustrated in Fig. 7 and Fig. 8.

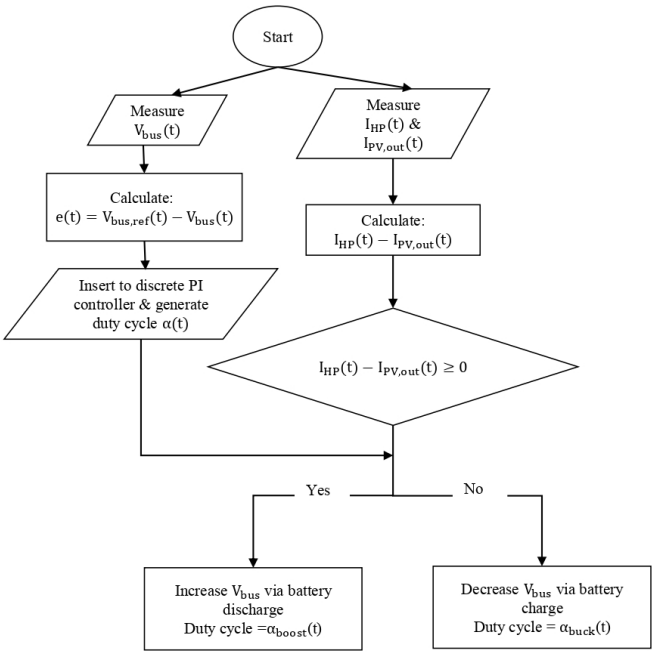

Fig. 7. Buck/boost mode algorithm of the BESS bidirectional converter.

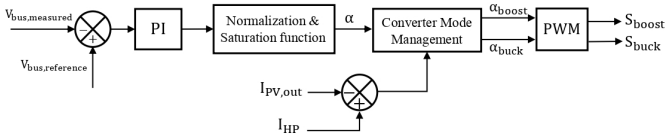

Fig. 8. PWM control signals for the buck and boost switches of the BESS bidirectional converter.

IV. RESULTS AND DISCUSSION

The system configuration previously defined in Fig. 1 was simulated in MATLAB/Simulink to validate the configuration under realistic operating conditions. Table I lists the parameters used in the simulation. The model was executed using a constant integration step of 10 μs, with the control loops updated at a switching rate of 10 kHz.

Fig. 9(a) illustrates the performance of the DC–bus voltage control system under varying operating conditions involving both PV generation and bidirectional BESS operation. The DC–bus voltage reached its 1000 V setpoint in about 4.46 s and stabilized within the ±5% band after roughly 0.75 s, demonstrating a rapid transient response. After settling, the voltage remained stable around the reference, with a mean value of 1000.11 V, and a root mean square error (RMSE) of 1.42%, confirming high precision during steady-state operation. Although brief overshoots were observed during operation, the system recovered quickly and, therefore, the overall operation of the system was not affected.

Fig. 9(b) illustrates the performance of the PV current control loop described in Section III. The measured PV-side inductor current meticulously tracked its reference throughout the operating period. The regular oscillations reflect dynamic irradiance input, and the controller responded quickly, maintaining a tight tracking with an RMSE of only 0.57 A, which confirms the precision and responsiveness of the controller. The minor mismatches observed occurred primarily during abrupt peaks in current demand but remain brief, indicating good transient behavior and system stability. These results validate the effectiveness of the proposed MPPT and current control scheme in ensuring accurate regulation of PV output and robust performance under varying solar conditions.

The energy management between the PV, the BESS and the two SWHPs is illustrated in Fig. 10 over an approximately 550-second simulation period. During high-irradiance periods exceeding 600 W/m^2, combined with the responsiveness of the MPPT and current control, the PV array delivered power above its nominal rating of 31 kW, with peaks approaching 35 kW. In particular, this occurred between 312–313 s, and between 527–529 s. Such transient overshoots are common in PV systems with variable solar input and reflect optimal energy extraction under dynamic conditions.

On the other hand, the electrical power demand of the SWHPs is intermittent, varying between 0 and 52 kW, reflecting the dynamics of the thermal load profile, previously shown in Fig. 3. The BESS operated bidirectionally, charging (negative power values) when the load demand is low, and discharging

(positive power values) when the load demand exceeds the PV generation, as illustrated in Fig. 10(b). The BESS provided up to 45 kW to maintain power balance. Furthermore, the overall power balance RMSE, which compares the combined generation of PV and BESS with the electrical demand of the SWHPs (Fig. 10(c)), was almost 6 kW, indicating effective coordination between components of the system.

The key performance metrics of the proposed control strategy are presented in Table II.

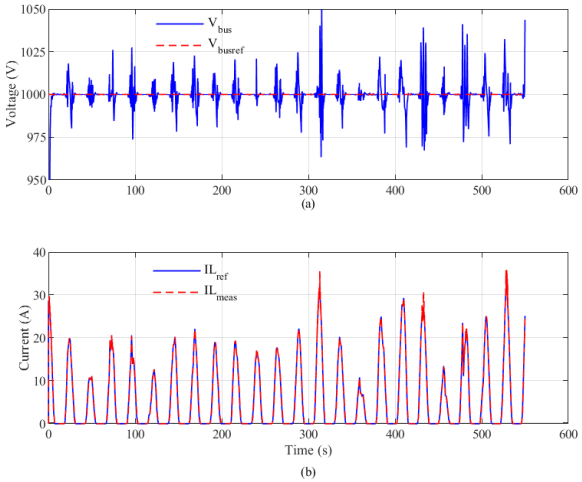

Fig. 9. Comparison of measured and reference (a) DC–bus voltage; (b) PV current output during control operation.

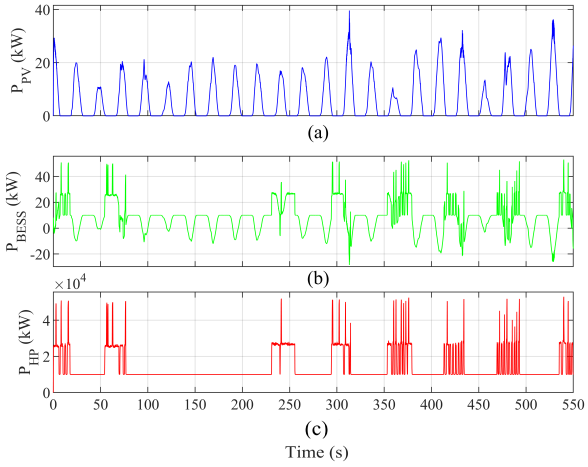

Fig. 10. Instantaneous power profiles of (a) the PV; (b) the BESS; and (c) the SWHPs.

V. Conclusion and Future Work

In this study, a hybrid system comprising a photovoltaic (PV) array, a battery energy storage system (BESS), and two parallel surface water heat pumps (SWHPs) was developed. The components and their associated models were described in detail and customized control methods were applied. The simulation results showed that the proposed strategy achieved a fast dynamic response, stable voltage regulation, and accurate power-tracking performance. The study demonstrated the feasibility and effectiveness of hybrid PV–BESS–SWHPs configurations for sustainably powering thermal systems, offering scalable and site-adaptable solutions. These findings confirm the objectives outlined in Section I, namely simulation of the hybrid system, improved MPPT, dual-loop BESS control, and performance evaluation under realistic operating conditions. Future work will focus on evaluating system performance with alternative DC–DC converter topologies, each governed by tailored control strategies.

TABLE I. SIMULATION PARAMETERS

Simulation parameters	Values
PV Module – Canadian Solar Inc. CS6X-350M-FG	
P_{MPPT}: Power at maximum power point	350 W
I_{MPPT}: Current at maximum power point	9.14 A
V_{MPPT}: Voltage at maximum power point	38.3 V
I_{sc}: Short-circuit current	9.67 A
V_{oc}: Open-circuit voltage	46.6 V
k_{sc}: Temperature coefficient of I_{sc}	0.048397 %/°C
k_{oc}: Temperature coefficient of V_{oc}	-0.3181 %/°C
PV's Boost Converter	
$C_{\mathrm{in,PV}}$: Input capacitance	180 μF
$C_{\mathrm{out,PV}}$: DC–bus capacitance	3300 μF
L_{PV}: Input inductance	1 mH
BESS – Lithium-Ion	
V_{nom}: Nominal Voltage	350 V
Ah: Rated Capacity	100 Ah
BESS's Buck–Boost Converter	
$C_{\mathrm{out,BESS}}$: DC–bus capacitance	3300 μF
L_{BESS}: Inductance	1 mH
$R_{\mathrm{L,BESS}}$: Inductor's resistance	10 mΩ
Other parameters	
T_{s}: Sampling time	10 μs
f: Switching frequency	10 kHz

TABLE II. Control Performance Metrics

Metric	Value
RMS voltage tracking error of DC–bus voltage	1.42%
Settling time of DC–bus voltage	0.75 s
PV current tracking RMSE	0.57 A
Power balance RMSE	6.026 kW

Acknowledgment

This work was carried out at the GREAH laboratory, University of Le Havre Normandie, particularly by the renewable energies and storage systems (MERS) team, within the framework of the Interreg Waterwarmth project, co-funded by the European Union. The authors would like to thank the European Union and the University of Le Havre Normandie for their financial support.

References

[1] International Energy Agency (IEA), "The future of heat pumps", Accessed: Sep. 22, 2025. [Online]. Available: https://www.iea.org/reports/the-future-of-heat-pumps/executive-summary, Nov. 2022.

[2] Deltares, "Aquathermal energy: Heating and cooling with water", Accessed: Jul. 8, 2025. [Online]. Available: https://www.deltares.nl/en/expertise/areas-of-expertise/energy-transition/aquathermal-energy, 2025.

[3] N. Damianakis, G. R. C. Mouli, and P. Bauer, "Grid impact of photovoltaics, electric vehicles and heat pumps on distribution grids—an overview", *Appl. Energy*, vol. 380, p. 125 000, 2025. DOI: 10.1016/j.apenergy.2025.125000.

[4] International Energy Agency (IEA), "District heating", Accessed: Jul. 8, 2025. [Online]. Available: https://www.iea.org/energy-system/buildings/district-heating, 2025.

[5] A. V. Klokov, A. S. Tutunin, E. S. Sharaborova, A. A. Korshunov, and E. Y. Loktionov, "Inverter heat pumps as a variable load for off-grid solar-powered systems", *Energies*, vol. 16, no. 16, p. 5987, 2023. DOI: 10.3390/en16165987.

[6] J. Rieck, L. Taube, and F. Behrendt, "Feasibility analysis of a heat pump powered by wind turbines and PV applications for detached houses in Germany", *Renew. Energy*, vol. 162, pp. 1104–1112, 2020. DOI: 10.1016/j.renene.2020.07.011.

[7] C. Charalambous, C. Heracleous, A. Michael, and V. Efthymiou, "Hybrid AC–DC distribution system for building integrated photovoltaics and energy storage solutions for heating-cooling purposes: A case study of a historic building in Cyprus", *Renew. Energy*, vol. 216, p. 119 032, 2023. DOI: 10.1016/j.renene.2023.119032.

[8] C. B. N. Fapi, M. L. Touré, M. B. Camara, and B. Dakyo, "High voltage gain DC–DC converter designed to extract maximum power from photovoltaic systems for heat-pump applications", in *Proc. 12th Int. Conf. Smart Grid (icSmartGrid)*, Setúbal, Portugal, 2024, pp. 493–498. DOI: 10.1109/icSmartGrid60512.2024.10620157.

[9] C. B. N. Fapi, M. L. Touré, M. B. Camara, and B. Dakyo, "MPPT-based fractional short-circuit current model predictive control for PV system in real weather conditions for heat-pump applications", in *Proc. 6th IEEE Int. Conf. Intell. Syst. Comput. Vis. (ISCV)*, Fez, Morocco, 2024, pp. 1–6. DOI: 10.1109/ISCV60512.2024.10620157.

[10] U. Chauhan, H. Chhabra, A. Rani, B. Kumar, and V. Singh, "An adaptive fractional order MPPT control for maximum power extraction from solar photovoltaic system", *Int. J. Adapt. Control Signal Process.*, vol. 39, 2025. DOI: 10.1002/acs.3988.

[11] M. A. Hannan et al., "Power electronics contribution to renewable energy conversion addressing emission reduction: Applications, issues, and recommendations", *Appl. Energy*, vol. 251, p. 113 404, 2019. DOI: 10.1016/j.apenergy.2019.113404.

[12] J. Assaf, J. S. Menye, M. B. Camara, D. Guilbert, and B. Dakyo, "Power converter topologies for heat pumps powered by renewable energy sources: A literature review", *Electronics*, vol. 13, no. 19, p. 3965, 2024. DOI: 10.3390/electronics13193965.

[13] C. B. Nzoundja Fapi, M. L. Touré, M. B. Camara, and B. Dakyo, "Control strategy for DC micro-grids in heat-pump applications with renewable integration", *Electronics*, vol. 14, no. 1, p. 150, 2025. DOI: 10.3390/electronics14010150.

[14] C. Lorenzo, L. Narvarte, R. H. Almeida, and A. B. Cristóbal, "Technical evaluation of a stand-alone photovoltaic heat-pump system without batteries for cooling applications", *Sol. Energy*, vol. 206, pp. 92–105, 2020. DOI: 10.1016/j.solener.2020.05.097.

[15] F. Nicoletti, G. Ramundo, and N. Arcuri, "Optimal operating strategy of hybrid heat pump–boiler systems with photovoltaics and battery storage", *Energy Convers. Manag.*, vol. 323, p. 119 233, 2025. DOI: 10.1016/j.enconman.2024.119233.

[16] M. B. Camara, "Supercapacitors for on-board dynamic energy exchange in hybrid-electric vehicles: Modeling, converter study, and control", Ph.D. dissertation, Univ. de Franche-Comté, Besançon, France, 2007.

[17] S. Agrawal, L. Umanand, and B. Subba Reddy, "Bidirectional current-fed converter for high gain DC–DC and DC–AC applications", in *Proc. Symp. Power Electron. Renew. Energy Syst. Control (PERESC)*, vol. 616, Bhubaneswar, India, 2021, pp. 101–111. DOI: 10.1007/978-981-16-1978-6_9.

[18] M. Louzazni and E. Aroudam, "Intelligent control of photovoltaic grid-connected using fuzzy logic based incremental conductance", *Procedia Technol.*, vol. 19, pp. 615–622, 2015. DOI: 10.1016/j.protcy.2015.02.087.